


Dilatometric insights into classical and modern maraging steels: a comparative analysis of grades 300, 350, and 400

Ana Larissa Melo Feitosa ^{1*} Daniela Passarelo Moura da Fonseca ¹ Leandro Gomes de Carvalho ² Angelo Fernando Padilha ¹ 

Abstract

Maraging steels feature prominently in the class of ultrahigh-mechanical-strength steels, achieving remarkable mechanical strength through an optimized combination of chemical compositions and a straightforward heat treatment process involving solution annealing and aging. In this study, the results acquired for the three main classes of maraging steels (300, 350, and 400), including grade 300 by additive manufacturing, using dilatometry complemented by other microstructural characterization techniques, such as scanning electron microscopy, transmission electron microscopy, Synchrotron X-ray diffraction, and Vickers hardness, are presented and compared. The main results obtained rely on the different dilatometric behaviors between grade 400 and the other grades (300 and 350). The former is characterized by lower Ni and higher Mo contents, appearing to present one main precipitate governing the increase in hardness before the occurrence of austenite reversion. The latter is primarily associated with two different precipitate types. The key conclusion drawn from this study is that varying the elemental ratios and production procedures play a pivotal role in the phase transformation of maraging steels, even suppressing the formation of Ni-rich phases and boosting the formation of Mo-rich phases.

Keywords: 18Ni maraging steels (300 and 350); 13Ni maraging steels (400); Dilatometry; Phase transformation; Additive manufacturing.

1 Introduction

Maraging steels are Fe-Ni-based steels characterized by a low C content and a martensitic matrix with a body-centered cubic crystal structure and lath morphology. This relatively soft and ductile matrix allows for processes such as cold rolling. The hardening of these steels occurs by the precipitation of nanometric intermetallic particles dispersed in the matrix during heat treatment, known as aging. Because of their high hardness, yield, and ultimate tensile strength, they are classified as ultrahigh-strength steels [1]. The most common grade of the steel is 18 wt. % Ni (maraging 250, 300, and 350) and 13 wt.% Ni (maraging 400), with distinct contents of Co, Mo, Ti, and Al additions [2-4].

The thermal cycle used for heat treatment is divided into two steps. Initially, solution annealing was conducted in the austenitic equilibrium phase field at approximately 820 °C, followed by air cooling. Subsequently, in the martensitic state, the aging step occurred at temperatures between 480 and 520 °C, lasting 3 to 5 h (10800 to 18000 s) for 18 wt.% Ni maraging steels (maraging 250, 300, and 350) [5]. Nevertheless, due to major Mo content, the solution annealing temperature range for maraging steel grade 400 is higher than that for 18%Ni maraging steels, covering between 1000 and 1250 °C [1].

During this last step, the precipitates nucleate and grow along the martensitic matrix, aided by pipe diffusion (diffusion along the dislocations). These precipitates are mainly Ni- and Mo-rich phases, such as Ni₃Ti, Ni₃Mo, and Fe₂Mo, with several morphologies and sizes [6-11]. At elevated temperatures and/or extended periods of aging, regions of Ni enrichment due to the loss of stability of Ni-type precipitates may induce austenite formation as reverted austenite [11-15]. Consequently, austenite formation, along with precipitate coarsening, results in a decrease in the mechanical strength of maraging steels, known as overaging [16,17].

In recent decades, maraging steels of grade 300 have been frequently produced using additive manufacturing. This term covers a wide range of techniques for progressively producing three-dimensional metal components layer-by-layer from a digital design [18]. One example is laser powder bed fusion (LPBF), also known as direct metal laser sintering (DMLS) or selective laser melting (SLM), which uses a focused laser to locally melt a layer of metal powder above an already solidified layer. The nonuniform heat distribution, repetitive melting, and rapid solidification cycles produced a microstructure comprising cellular growth in columnar grains that followed the heat direction. Consequently,

¹Departamento de Engenharia Metalúrgica e de Materiais, Universidade de São Paulo, USP, São Paulo, SP, Brasil.

²Centro Universitário Adventista de São Paulo, UNASP, São Paulo, SP, Brasil.

*Corresponding author: larissa.mfeitosa@gmail.com



segregation, residual tension, and retained austenite are common issues in maraging steels produced by additive manufacturing [18-20], requiring appropriate heat treatment to homogenize the microstructure. Maraging steels processed through LPBF have been used in the industry because of their ideal printability. However, there is still a demand for further studies, as the literature indicates that processing parameters, such as scanning velocity, hatch space, building direction, and post-processing heat treatments, significantly influence the microstructure and physical metallurgy of these materials [21-26].

In addition to studies analyzing the phase transformations in conventional or additively manufactured maraging steels through microstructural characterization, metallurgists have frequently employed dilatometry to study the phase transformations in maraging steels [27,28]. This technique is widely used because of its high precision and relative practicality. Its ease of use is based on the principle of measuring the linear thermal expansion of materials, which deviates from linearity when a phase transformation occurs. Therefore, it is possible to identify the start and end temperatures of the transformations based on the dilatometric curve behavior.

In this context, numerous studies related to the investigation of maraging steels or similar alloys that use dilatometry have been published, some of which used other methods along with dilatometry to study phase transformations [29-34], and some focused on this technique as the main source of information [35-38]. Nonetheless, dilatometry provides all these studies with sufficient bases to well characterize the phase transformations in the materials, from which they could, for example, find the temperatures of transformation [31,37], compare the dilation behavior with the phase quantification from other techniques [34], estimate phase quantification directly from the dilatometric curve, compare with other methods [36], and estimate time-temperature-transformation plots [35,38].

In this study, dilatometry and other complementary techniques were employed to track the precipitation behavior and martensite reversion into austenite in various types of maraging steel. The steels were produced using conventional manufacturing (grades 300, 350, and 400) and additive manufacturing (grade 300). The main motivation for this study was the lack of comparative studies in the literature encompassing the three most modern grades of maraging steels, with a predominant focus on using the same and widely adopted experimental technique: dilatometry.

2 Methodology

The maraging steels used in this study were commercial maraging steels of grades 300, 350, and 400 produced by casting and forging (labeled as 300F, 350F, 400F, and 400Lab, respectively) and maraging steel of grade 300 produced by additive manufacture (300AM). The 400Lab is a maraging steel grade 400 experimentally produced at the laboratory scale with distinct Mo and Ti contents. The chemical compositions of all the steels used are listed in Table 1. The chemical composition of 300F, 350F, 400F, and 400 Lab were provided by the supplier, Villares Metals S/A, and the composition of the as-built 300AM was measured by optical emission spectroscopy according to the ASTM A751 standard in a certified laboratory.

Maraging steels 300F and 350F were produced using vacuum induction melting (VIM) followed by vacuum arc remelting (VAR). In addition, 400F and 400Lab were produced using VIM and VAR, but had a further step of electroslag remelting. Subsequently, all ingots were hot forged and subsequently solution annealed (initial condition) at 820 °C for 3600 s for 300F and 350F and at 1000 °C for 3600 s for 400F and 400Lab to ensure a single homogenized martensitic phase.

The 300AM was manufactured through LPBF using maraging 300 powder from SLM Solutions in an EOS DMLS M280 machine at the *Instituto Nacional de Ciência e Tecnologia* (INCT), Unicamp, Brazil. The processing parameters were in accordance with the manufacturer's specifications [39].

Ar was purged in a machine chamber before material processing. The material was analyzed under the as-built condition (initial condition).

Dilatometric analyses were conducted on cylindrical samples measuring 4 mm in diameter and 10 mm in length, using a Bähr DIL 805 A/D dilatometer. The thermal cycle conducted was continuous heating up to 900 °C at a rate of 1 °C.s⁻¹. Furthermore, the experimental errors of 2 °C in the transformation temperatures determined by the linearity deviations of the dilatometric curve were estimated using the Pearson linear coefficient of determination and an analysis of the behavior of the experimental data around the linear fit using absolute residuals.

Microstructural characterization was performed using light optical microscopy (LOM) and scanning electron microscopy (SEM) with an FEG-SEM FEI Inspect 50 (EBSD

Table 1. Chemical composition of the maraging steels (wt.%)

	Ni	Co	Mo	Ti	Al	Cr	Si	Mn	C	Fe
300F	18.69	8.99	5.01	0.80	0.09	0.01	0.01	0.02	0.001	bal.
350F	17.85	12.10	4.80	1.40	0.10	0.04	0.02	0.03	0.005	bal.
400F	13.08	15.35	11.30	0.88	0.05	-	0.08	0.05	0.024	bal.
400Lab	14.06	15.21	15.02	0.24	0.04	-	0.06	0.04	0.021	bal.
300AM	18.82	8.8	4.46	1.45	0.06	0.17	0.08	0.02	0.008	bal.

bal. = balance.

analysis was performed for 350F), and transmission electron microscopy (TEM) with an FEG-TEM JEOL 2100F operated at 200 kV. SEM samples were prepared by polishing up to 1 μm diamond paste and etching with Nital 2% (2 mL nitric acid + 98 mL ethanol) for the maraging 300 and 350 ones and with Vilella's reagent (1 g picric acid, 5 mL HCl, and 100 mL ethanol) for the maraging 400 ones. TEM specimens were prepared by focused ion beam (FIB) using an FEI DualBeam Helios NanoLab 650 for the 400F samples and a Thermo Fisher Scientific Helios NanoLab 660 for the 350F samples. The Vickers hardness measurements were performed under a load of 1 kg for 15 s. The synchrotron X-ray diffraction (SXR) data of all samples were collected by single-shot in the beamline P07 PETRA III of the Deutsches Elektronen-Synchrotron (DESY) – Hamburg, Germany ($\lambda = 0,142350 \text{ \AA}$).

3 Results and discussion

Figure 1a presents the SXR patterns for the 300F, 350F, and 300AM samples at their initial conditions (solution annealed for 300F and 350F and as-built for the 300AM). Figure 1a compares the SXR patterns, showing 300AM in the as-built condition presented a retained austenite of approximately 7.06 vol. %, using the same quantification methodology of previous work [13] and considering the peaks $(200)\gamma$, $(200)\alpha'$, $(220)\gamma$, $(211)\alpha'$, and $(311)\gamma$. Small peaks of austenite, indicated by the black arrows, were found at 350F and quantified as less than 1 vol. %. Only one small austenite peak was observed at 300F; thus, this phase could not be quantified. Secondary phases, also known as precipitates, are indicated by orange arrows. The precipitate peaks match

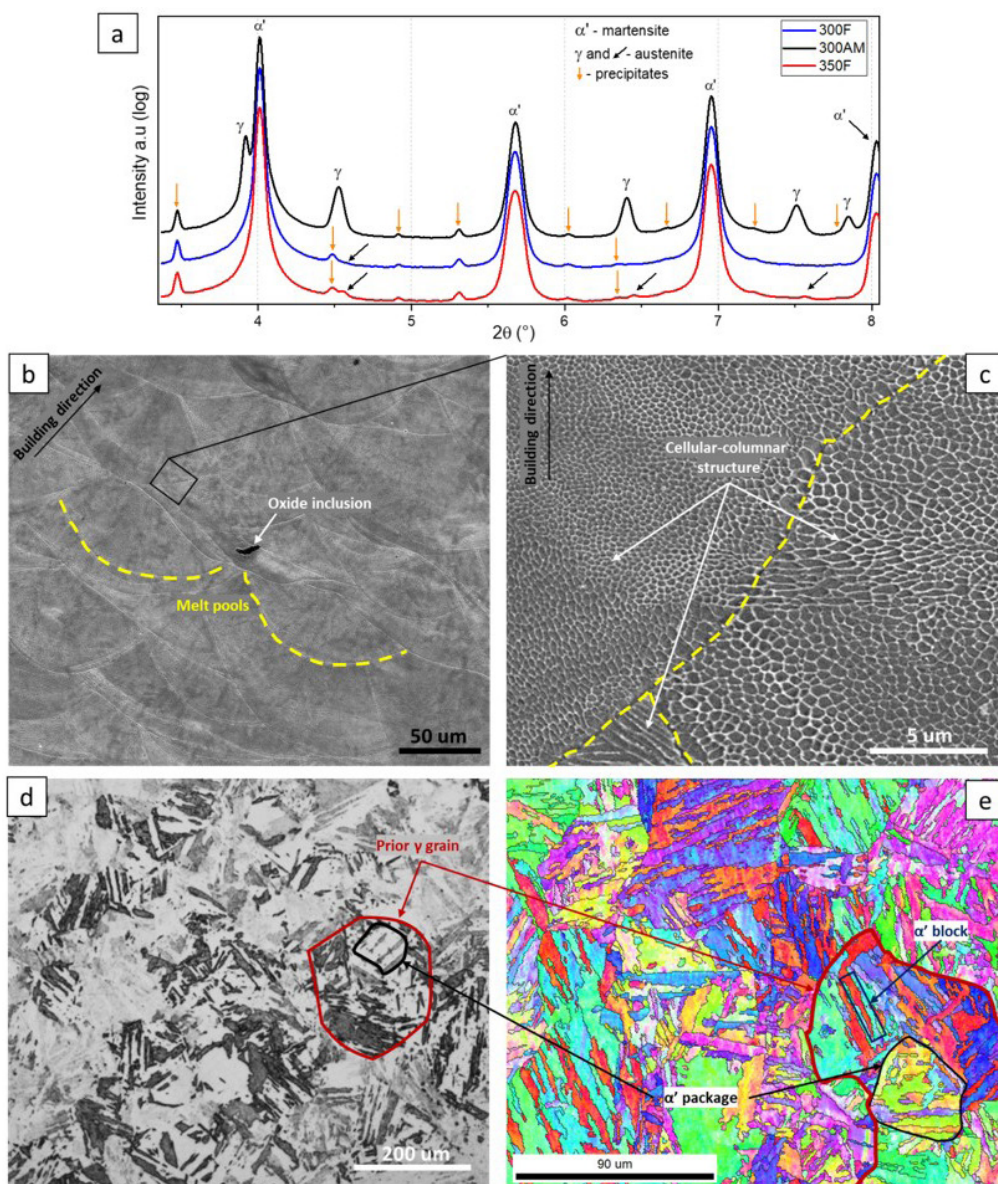


Figure 1. (a) SXR patterns for 300AM, 300F, and 350F at the initial condition, (b) SEM image of sample 300AM showing the melt pools microstructure, (c) SEM image of sample 300AM from the area indicated, (d) LOM image of 350F sample, and (e) EBSD image of 350F.

the superposed peaks of Ni_3Ti and Fe_2Mo , which originate from the production process, because the conventionally fabricated ones are forged at high temperatures and the subsequent 1 h solution annealing is not sufficient to dissolve all secondary phases. In contrast, additively manufactured 300AM was not solution-annealed, and secondary phases, oxides, and inclusions were common [40,41].

Figure 1b and c show SEM images of the 300AM, presenting the as-built manufactured microstructure with the melt-pool contours (some indicated by the dashed yellow lines) and the cellular-columnar growth microstructure, respectively. Some authors have confirmed that retained austenite occurs between cellular boundaries [41,42]. Figure 1d and 1e present light optical microscopy and EBSD images, respectively, of the 350F sample. The red contour in both figures indicates a probable prior austenite grain, and the black contour depicts a package of lath martensite. The blue rectangle in Figure 1e illustrates a lath martensite block. The block/package martensitic organization of maraging steels has been previously studied [1,33,43].

The dilatometric curves of the 300F, 350F, and 300AM for the continuous heat treatment ($1\text{ }^\circ\text{C}\cdot\text{s}^{-1}$ up to

$900\text{ }^\circ\text{C}$) are illustrated in Figure 2. A more detailed view and the derivative curves for each material are shown in Figure 2b. Notably, there is a loss of linearity associated with the precipitation process, as indicated in the graph. Additionally, other changes in linearity are observed for all materials around $700\text{ }^\circ\text{C}$, corresponding to the formation of reverted austenite. In the cases of 300F and 350F, a third nonlinear behavior, which is related to the reverted austenite transformation governed by shear, was observed [35-37].

This latter phenomenon was not detected for the 300AM due to its occurrence just at a heating rate below $15\text{ }^\circ\text{C}/\text{min}$ as found by Król et al. [44] in a study of a similar additive manufactured by maraging 300 steel.

To illustrate the phases found in those maraging steels, Figure 2c and Figure 2d depict the reverted austenite formed in 350F after overaging at $600\text{ }^\circ\text{C}$ for 3600 s and in 300AM after aging at $480\text{ }^\circ\text{C}$ for 18000 s, respectively. Figure 2e shows the two main precipitates (Ni_3Ti and Fe_2Mo) found in 350F after aging at $600\text{ }^\circ\text{C}$ for 1800 s.

The results for the 400 maraging steels are shown in Figure 3. Figure 3a shows the SXRD patterns of the 400F and 400Lab samples under the initial conditions. The orange

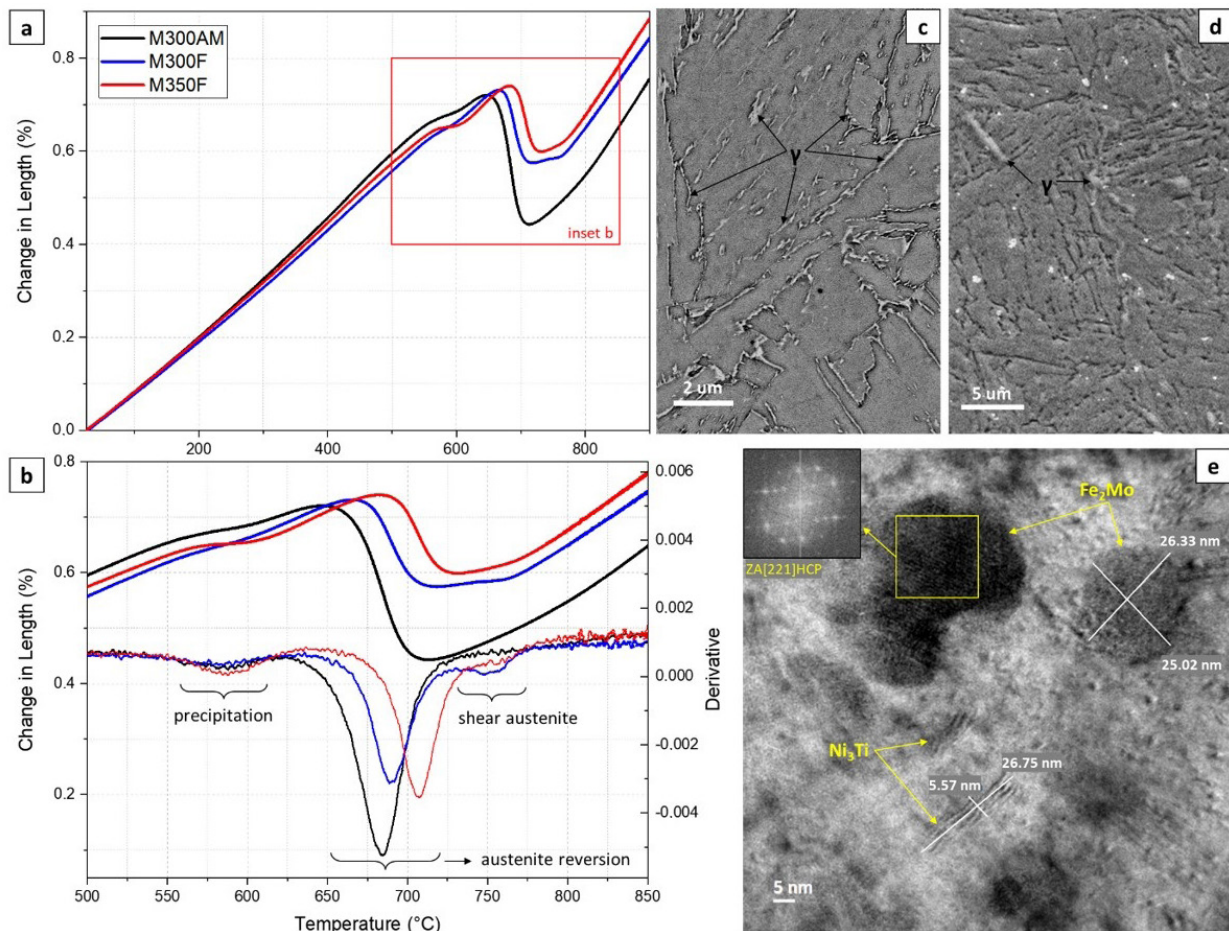


Figure 2. (a) Dilatometric curves of 300AM, 300F and 350F, (b) Selected area in (a) along with the derivative graphics, (c) SEM image of 350F (aged at $600\text{ }^\circ\text{C}$ for 3,600 s) showing the reverted austenite, (d) SEM image of 300AM (aged at $480\text{ }^\circ\text{C}$ for 18,000 s) showing the reverted austenite, and (e) TEM image with precipitates found in 350F after aging ($600\text{ }^\circ\text{C}$ for 1,800 s).

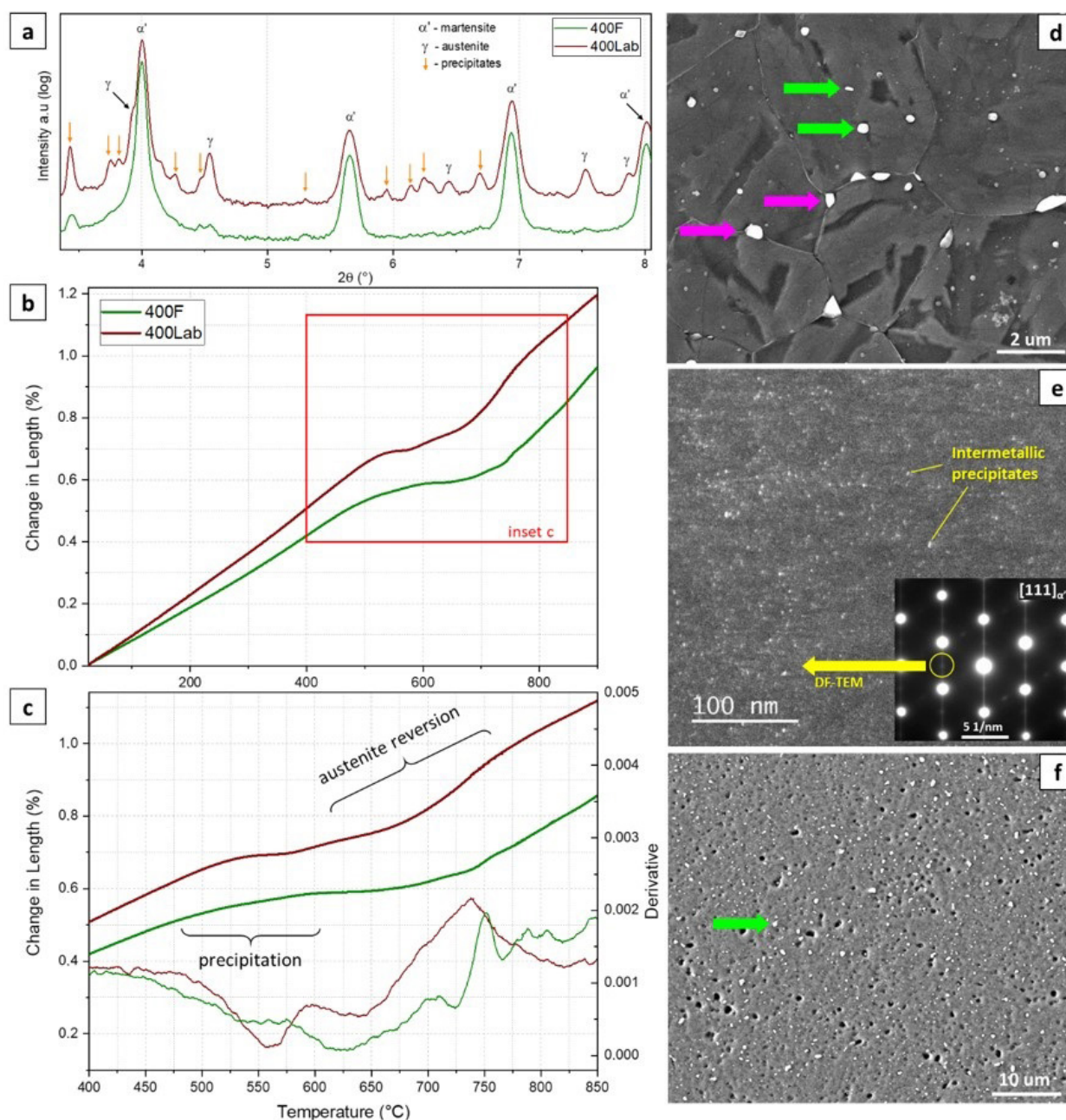


Figure 3. (a) SXRDR patterns for samples 400F and 400Lab at the initial solution annealed condition, (b) Dilatometric curves of 400F and 400Lab samples, (c) Selected area in (b) along with the derivative graphics, (d) SEM image of sample 400F at the initial condition; the pink arrows shows micrometric precipitates at the prior austenite grain boundary and green arrows indicates smaller micrometric precipitates inside the grain, (e) DF-TEM image of sample 400F, the nanometric intermetallic precipitates are in light gray contrast distributed throughout the matrix, (inset: SAED pattern along [111] direction of matrix indicating the spot that DF-TEM image was generated), and (f) SEM image of sample 400Lab at the initial condition.

and blue arrows indicate an estimation of the Fe_2Mo and Fe_7Mo_6 peaks; the α' symbols indicate the martensitic matrix peaks, and the γ symbols the austenite ones. The exact identification and differentiation of the precipitates is difficult because these phases have numerous overlapping peaks and similar crystallographic structures. In addition, the major presence of retained austenite was due to the higher content of austenite-stabilizing elements (Ni and Mo) in the 400Lab material than in the 400F material [45].

Figure 3b and c illustrate the dilatometric curves of the 400F and 400Lab for the continuous heat treatment ($1^\circ\text{C}\cdot\text{s}^{-1}$ up to 900°C). Figure 3c shows the derivative curves of each of the 400 maraging steels.

During heating, expansion was uniformly continuous until the start of austenite (As) reversion, which occurred at $645 \pm 2^\circ\text{C}$ and $650 \pm 2^\circ\text{C}$ for 400F and 400Lab, respectively. Austenite (Af) reversion ended at $842 \pm 2^\circ\text{C}$ and $828 \pm 2^\circ\text{C}$, respectively. Although the 400Lab sample

had a higher Ni content than 400F, the austenite reversion started at practically the same temperature for both samples because of the heterogeneous distribution of nickel in the retained austenite in 400Lab (Figure 3a). Furthermore, this effect was observed for temperature A_f for both samples.

The SEM image of 400F in the initial condition (solution-annealed) is shown in Figure 3d. The presence of micrometric precipitates (with approximately 0.5 μm mean diameter) at the prior austenite grain boundary (pink arrows) and inside the grains (green arrows), with approximately 0.1 μm mean diameter, is notable. These precipitates on the annealed material can contribute to some hardness increase by dispersion hardening mechanisms; however, the main reason for the ultrahigh strength of maraging steels is the nanometer-sized intermetallic precipitates formed during aging. Figure 3e shows a dark-field TEM (DF-TEM) image and a selected-area electron diffraction (SAED) pattern, indicating the spot that generated the image. The intermetallic precipitates presented in Figure 3e (small dots in light gray contrast) were formed during aging heat treatment at 480 °C for 3 h. Previous work from this research group indicated that the intermetallic precipitates in samples with a base composition of maraging 400 were Fe_2Mo [9]. Figure 3f shows the SEM image of 400Lab under the initial solution-annealed condition. Because of its high Mo content, 400Lab contains a higher density of micrometric precipitates (green arrow) and does not present the characteristic morphology of lath martensite.

The effect of chemical composition on the transformation temperatures for all materials obtained from the dilatometric curves is summarized in Table 2. The 300F and 300AM materials presented higher start (Ps) and finish (Pf) precipitation temperatures because of the lower amount of Co present in these samples compared with maraging 350 and 400 steels [1,8,37,46]. Furthermore, the Ps temperature at 300AM was lower than that observed at 300F, indicating that the heterogeneous distribution of Ni may have favored the formation of Ni-type precipitates. The fact that maraging 400 steels have a higher content of Mo and Co results in more pronounced and accelerated precipitation owing to the synergistic effect between these two elements in the formation of precipitates, which can be seen in the lower Ps temperatures for the 400Lab and 400F samples [1,46].

Table 2 also shows a comparison of the austenite reversion temperatures, As and Af, of the analyzed maraging

steel samples. Although the 400F and 400Lab samples contained higher amounts of Co than the 300F sample, they had austenite reversion temperatures, As, close to 650 °C, indicating that the increase in the content of precipitate-forming elements for maraging steels, such as Mo, also led to a reduction in the As temperature [1,45]. In addition, the 350F sample had a higher As temperature than the 300F maraging steel because of the presence of a higher Co content, which delayed the onset of the reversion of martensite [45,46]. Furthermore, sample 300AM exhibited the lowest As temperature among all the analyzed samples. This can be attributed to the heterogeneous distribution of Ni, which accelerates the reversion of martensite [19,46]. Additionally, under the initial condition, the 300AM had retained austenite, potentially acting as a nucleation site and facilitating austenite reversion [43].

Nonetheless, the transformation temperatures are dependent on the steel chemical composition and heating/cooling rates; therefore, caution is required when comparing the aforementioned temperatures with other studies. For example, specifically, some authors calculated the reverted austenite transformation temperatures for maraging steel grade 400, that is, Hornbogen and Rittner [3], Menzel and Klaar [4], and Padial [47].

According to Hornbogen and Rittner [3], after heating a 13Ni-15Co-10-Mo maraging steel up to 900 °C at heating and cooling rates of 2 °C.min⁻¹ (0.0333 °C.s⁻¹), they found the mean As and Af to be 656.5 °C and 823 °C, respectively. Mean values were calculated based on two measurements. Comparing these temperatures with the ones found to the 400F sample (same composition used by Hornbogen and Rittner) heated at 1 °C.s⁻¹, the higher heating rate makes the reverted austenite start at 11 °C lower and end at around 9 °C higher. This indicates that the nucleation of reverted austenite could be delayed by the lower heating rate owing to the higher precipitation stability of the maraging 400 steel when compared to the maraging 300 and 350 steels under the microstructural conditions studied. Consequently, the growth of reverted austenite is delayed because the diffusion-controlled transformation requires time to occur completely.

Figure 4 illustrates the effect of the chemical composition in response to the aging treatment for the maraging 300, 350, and 400 steels by the Vickers hardness measurements in samples aged at 480 °C. The Vickers hardness values of the maraging 350 steel are higher than those of the maraging

Table 2. Transformation temperatures of all samples

	Ps (°C)	Pf (°C)	As (°C)	Af (°C)
300F	548	612	649	785
300AM	498	614	632	806
350F	488	623	658	807
400F	466	606	645	842
400Lab	460	602	650	828

Ps = precipitation start temperature; Pf = precipitation finish temperature; As = austenite start temperature; Af = austenite finish temperature. (Estimated error ± 2 °C).

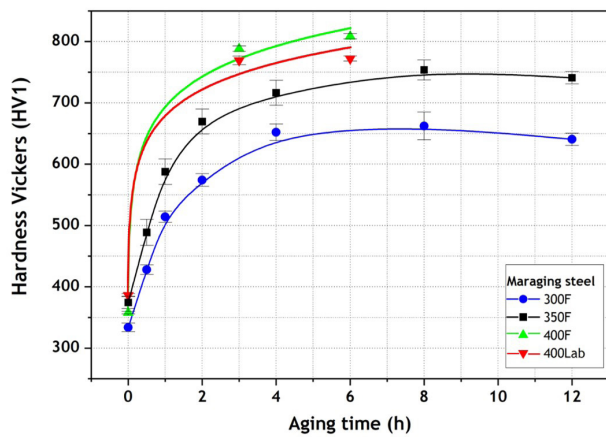


Figure 4. Vickers Hardness evolution curves of 300F, 350F, 400F and 400Lab materials aged at 480 °C.

300 steel owing to the higher Co content, which decreases the Mo solubility [1,8,37,46]. Furthermore, the Vickers hardness values of maraging steel 400 were higher than those of the maraging grades 300 and 350. In addition to the close values of hardness at the initial condition for 400F and 400Lab samples, after 3 h of aging, they achieved hardness of 788 ± 4 HV and 769 ± 7 HV, respectively, while the maximum hardness of samples 300F and 350F were 662 ± 22 HV and 753 ± 16 HV, respectively, for longer aging times. The higher hardness achieved by maraging steel 400 is mainly due to the increase in the Mo and Co contents, which causes a higher density of nanometric precipitates [48].

In addition to the influence of the composition on the precipitate density, the composition can cause changes in the precipitate type [9,49]. Studies on the precipitation of maraging 300 have reported the presence of Ni_3Mo precipitates, while affirming that the main reason for the higher strength and hardness of maraging 400 is associated with the Fe_2Mo precipitate [22,31,50-52]. Although, the carbon content on maraging 400 is greater than the other grades, this does not imply nor justifies directly the higher hardness values of this grade. The carbon as residual element, as well as N and S, are stabilized, during the steel making process, with Ti which allows the production of $Ti(C,N)$, $(Ti,Mo)C$ and $Ti_4C_2S_2$. These precipitates present themselves in sizes between 1 to 15 μm , and very low volume fraction in the matrix. This way, the carbides and/or carbo-sulfides do not have significant influence on the material hardening process when compared to the intermetallic precipitates generated during the hardening heat treatments [53-56].

4 Conclusions

Maraging steels of grades 300, 350, and 400 were compared using several techniques, primarily dilatometry; some aspects are worth highlighting.

- Dilatometry is an adequate technique for analyzing the effects of the chemical composition and production process on the phase transformation of conventional and additively manufactured maraging steels;
- Conventionally produced maraging steel grades 300 and 350 have similar dilatometric curve behaviors because they present three distinct steps of phase transformation: related to precipitation as a slight contraction, reverted austenite formed via diffusion as a large contraction, and shear-controlled austenite. Although these transformations occur at distinct start and end temperatures;
- The production process of maraging steels grade 300 plays an important role in phase transformations because the additive manufacturing technique creates a microstructure rich in segregation and retained austenite compared to those manufactured using conventional methods;
- Maraging steel grade 400 has a distinct dilatometric behavior compared to the other grades, even though they all share the same alloy elements in different proportions. The lower amount of Ni and higher amounts of Mo and Co caused the precipitation to occur at a lower temperature and made this step full of Mo-rich precipitates because Ni-rich precipitates were not detected;
- The earlier precipitation made the 400 samples present a higher hardness peak than the 300 and 350 ones, showing that maybe the Mo-rich precipitates have a more effective role in rising the hardness;
- The distinct Vickers hardness values achieved by the different maraging steels studied were associated with the density, morphology, and nature of the precipitates in each material. Thus, the smaller amount of Ti in 300F led to fewer precipitates and, thus, lower hardness values, whereas the homogeneous distribution of spherical Mo-rich precipitates in 400F led to the highest hardness values among the studied materials.

Acknowledgements

This study was financed in part by the National Council for Scientific and Technological Development (CNPq) – grant number 168256/2018-5 – and by the Coordenação de Aperfeiçoamento de Pessoal de Nível Superior – Brasil (CAPES) – Finance Code 88887.570306/2020-00 and 88887.485335/2020-00. The authors would like to thank Professor Julian Avila for providing the additive manufactured material. Work at the Molecular Foundry was supported by the Office of Science, Office of Basic Energy Sciences, of the U.S. Department of Energy under Contract No. DE-AC02-05CH11231. The authors would

like to acknowledge the National Institute of Metrology, Standardization and Industrial Quality (INMETRO). We acknowledge DESY (Hamburg, Germany), a member of the Helmholtz Association HGF, for the provision of experimental facilities. Parts of this research were carried out at PETRA III and we would like to thank Dr. Norbert Schell and Dr. Emad Maawad for assistance in using P07 - High Energy Materials Science. Beamtime was allocated

for proposal I-20211036. The authors would like to thank Dr. Maria Virginia Pires Altoé (Molecular Foundry – Lawrence Berkeley National Laboratory), Dr. Braulio S. Archanjo (Divisão de Metrologia de Materiais – Instituto Nacional de Metrologia, Qualidade e Tecnologia), Dr. Emilia Annese (Brazilian Center for Physics Research). We would like to thank Editage (www.editage.com.br) for English language editing.

References

- 1 Fonseca DPM, Feitosa ALM, Carvalho LG, Plaut RL, Padilha AF. A short review on ultra-high-strength maraging steels and future perspectives. *Materials Research*. 2021;24(1):e20200470. <http://doi.org/10.1590/1980-5373-mr-2020-0470>.
- 2 Rohrbach K, Schmidt M. Maraging steels. In: ASM Handbook Committee, editor. *Properties and selection: irons, steels, and high-performance alloys*. Vol. 1. Materials Park: ASM International; 1990. p. 793-800. <http://doi.org/10.31399/asm.hb.v01.a0001043>.
- 3 Hornbogen E, Rittner K. Development of thermo-mechanical treatments of a maraging steel for yield strengths above 3 GPa. *Steel Research*. 1987;58(4):172-177. <http://doi.org/10.1002/srin.198700857>.
- 4 Menzel J, Klaar H-J. Systematische Gefügeuntersuchungen am martensitaushärtenden Stahl X 2 NiCoMo 13 15 10. *Steel Research*. 1990;61:30-38. <http://doi.org/10.1002/srin.199000293>.
- 5 Schmidt M, Rohrbach K, Carson C. Heat treating of maraging steels. In: ASM Handbook Committee, editor. *Heat treating of irons and steels*. Vol. 4. Materials Park: ASM International; 2014. p. 468-80. <http://doi.org/10.31399/asm.hb.v04d.a0005948>.
- 6 Sha W, Leitner H, Guo Z, Xu W. Phase transformations in maraging steels. In: Pereloma E, Edmonds DV, editors. *Phase transformations in steels*. Burlington: Elsevier; 2012, p. 332-362. <http://doi.org/10.1533/9780857096111.2.332>.
- 7 Xu X, Ganguly S, Ding J, Guo S, Williams S, Martina F. Microstructural evolution and mechanical properties of maraging steel produced by wire + arc additive manufacture process. *Materials Characterization*. 2018;143:152-162. <http://doi.org/10.1016/j.matchar.2017.12.002>.
- 8 Peters DT, Cupp CR. The kinetics of ageing reactions in 18%Ni maraging steels. *Trans AIME*. 1966;236:1420-1429.
- 9 Fonseca DPM, Altoé MVP, Archanjo BS, Annese E, Padilha AF. Influence of Mo content on the precipitation behavior of 13Ni maraging ultra-high strength steels. *Metals*. 2023;13(12):1929. <http://doi.org/10.3390/met13121929>.
- 10 Carvalho LG, Plaut RL, Padilha AF. Precipitation kinetic analysis in a Maraging 350 steel using KJMA and Austin-Rickett equations. *Defect and Diffusion Forum*. 2022;420:118-128. <http://doi.org/10.4028/p-luf4h8>.
- 11 Moshka O, Pinkas M, Brosh E, Ezersky V, Meshi L. Addressing the issue of precipitates in maraging steels: unambiguous answer. *Materials Science and Engineering A*. 2015;638:232-239. <http://doi.org/10.1016/j.msea.2015.04.067>.
- 12 Rohit B, Muktinatalapati NR. Austenite reversion in 18% Ni maraging steel and its weldments. *Materials Science and Technology*. 2018;34(3):253-260. <http://doi.org/10.1080/02670836.2017.1407544>.
- 13 Feitosa ALM, Escobar J, Ribamar GG, Avila JA, Padilha AF. Direct Observation of Austenite Reversion During Aging of 18Ni (350 Grade) Maraging Steel Through In-Situ Synchrotron X-Ray Diffraction. *Metallurgical and Materials Transactions. A, Physical Metallurgy and Materials Science*. 2022;53(2):420-431. <http://doi.org/10.1007/s11661-021-06496-y>.
- 14 Li X, Yin Z. Reverted austenite during aging in 18Ni(350) maraging steel. *Materials Letters*. 1995;24(4):239-242. [http://doi.org/10.1016/0167-577X\(95\)00109-3](http://doi.org/10.1016/0167-577X(95)00109-3).
- 15 Carvalho LG, Plaut RL, de Lima NB, Padilha AF. Kinetics of martensite reversion to austenite during overaging in a maraging 350 steel. *ISIJ International*. 2019;59(6):1119-1127. <http://doi.org/10.2355/isijinternational>. ISIJINT-2018-610.
- 16 Viswanathan UK, Dey GK, Sethumadhavan V. Effects of austenite reversion during overageing on the mechanical properties of 18 Ni (350) maraging steel. *Materials Science and Engineering A*. 2005;398(1-2):367-372. <http://doi.org/10.1016/j.msea.2005.03.074>.

- 17 Pardal JM, Tavares SSM, Terra VF, Silva MR, Santos DR. Modeling of precipitation hardening during the aging and overaging of 18Ni-Co-Mo-Ti maraging 300 steel. *Journal of Alloys and Compounds*. 2005;393(1-2):109-113. <http://doi.org/10.1016/j.jallcom.2004.09.049>.
- 18 DebRoy T, Wei HL, Zuback JS, Mukherjee T, Elmer JW, Milewski JO, et al. Additive manufacturing of metallic components: process, structure and properties. *Progress in Materials Science*. 2018;92:112-224. <http://doi.org/10.1016/j.pmatsci.2017.10.001>.
- 19 Conde FF, Avila JA, Oliveira JP, Schell N, Oliveira MF, Escobar JD. Effect of the as-built microstructure on the martensite to austenite transformation in a 18Ni maraging steel after laser-based powder bed fusion. *Additive Manufacturing*. 2021;46:102122. <http://doi.org/10.1016/j.addma.2021.102122>.
- 20 Mooney B, Kourousis K. A review of factors affecting the mechanical properties of maraging steel 300 fabricated via laser powder bed fusion. *Metals*. 2020;10(9):1273. <http://doi.org/10.3390/met10091273>.
- 21 Tekin T, Ischia G, Naclerio F, Ipek R, Molinari A. Effect of a direct aging heat treatment on the microstructure and the tensile properties of a 18Ni-300 maraging steel produced by Laser Powder Bed Fusion. *Materials Science and Engineering A*. 2023;872:144921. <http://doi.org/10.1016/j.msea.2023.144921>.
- 22 Mao Z, Lu X, Yang H, Niu X, Zhang L, Xie X. Processing optimization, microstructure, mechanical properties and nanoprecipitation behavior of 18Ni300 maraging steel in selective laser melting. *Materials Science and Engineering A*. 2022;830:142334. <http://doi.org/10.1016/j.msea.2021.142334>.
- 23 Shamsdini S, Pirgazi H, Ghoncheh MH, Sanjari M, Amirkhiz BS, Kestens L, et al. A relationship between the build and texture orientation in tensile loading of the additively manufactured maraging steels. *Additive Manufacturing*. 2021;41:101954. <http://doi.org/10.1016/j.addma.2021.101954>.
- 24 Vishwakarma J, Chattopadhyay K, Santhi Srinivas NC. Effect of build orientation on microstructure and tensile behaviour of selectively laser melted M300 maraging steel. *Materials Science and Engineering A*. 2020;798:140130. <http://doi.org/10.1016/j.msea.2020.140130>.
- 25 Patil VV, Mohanty CP, Prashanth KG. Selective laser melting of a novel 13Ni400 maraging steel: Material characterization and process optimization. *Journal of Materials Research and Technology*. 2023;27:3979-3995. <http://doi.org/10.1016/j.jmrt.2023.10.193>.
- 26 Peinado G, Carvalho C, Jardim A, Souza E, Avila JA, Baptista C. Microstructural and mechanical characterization of additively manufactured parts of maraging 18Ni300M steel with water and gas atomized powders feedstock. *International Journal of Advanced Manufacturing Technology*. 2024;130(1-2):223-237. <http://doi.org/10.1007/s00170-023-12686-2>.
- 27 Chevenard MP. Mécanisme de la trempe des aciers au carbone. *Revue de Métallurgie*. 1919;16(1-2):17-80. <http://doi.org/10.1051/metal/191916010017>.
- 28 Wells C, Ackley RA, Mehl RF. A dilatometric study of the α - γ transformation in high-purity iron. *Transactions of the American Society for Metals*. 1936;24:46-66.
- 29 Ooi SW, Hill P, Rawson M, Bhadeshia HKDH. Effect of retained austenite and high temperature Laves phase on the work hardening of an experimental maraging steel. *Materials Science and Engineering A*. 2013;564:485-492. <http://doi.org/10.1016/j.msea.2012.12.016>.
- 30 Viswanathan UK, Dey GK, Asundi MK. Precipitation hardening in 350 grade maraging steel. *Metallurgical Transactions. A, Physical Metallurgy and Materials Science*. 1993;24(11):2429-2442. <http://doi.org/10.1007/BF02646522>.
- 31 He Y, Yang K, Qu W, Kong F, Su G. Strengthening and toughening of a 2800-MPa grade maraging steel. *Materials Letters*. 2002;56(5):763-769. [http://doi.org/10.1016/S0167-577X\(02\)00610-9](http://doi.org/10.1016/S0167-577X(02)00610-9).
- 32 Conde FF, Escobar JD, Oliveira JP, Jardim AL, Bose WW Fo, Avila JA. Austenite reversion kinetics and stability during tempering of an additively manufactured maraging 300 steel. *Additive Manufacturing*. 2019;29:100804. <http://doi.org/10.1016/j.addma.2019.100804>.
- 33 Loewy S, Rheingans B, Meka SR, Mittemeijer EJ. Unusual martensite-formation kinetics in steels: observation of discontinuous transformation rates. *Acta Materialia*. 2014;64:93-99. <http://doi.org/10.1016/j.actamat.2013.11.052>.
- 34 Escobar JD, Oliveira JP, Salvador CAF, Tschiptschin AP, Mei PR, Ramirez AJ. Double-step inter-critical tempering of a supermartensitic stainless steel: Evolution of hardness, microstructure and elemental partitioning. *Materials Characterization*. 2019;158:109994. <http://doi.org/10.1016/j.matchar.2019.109994>.
- 35 Kapoor R, Batra IS. On the α to γ transformation in maraging (grade 350), PH 13-8 Mo and 17-4 PH steels. *Materials Science and Engineering A*. 2004;371(1-2):324-334. <http://doi.org/10.1016/j.msea.2003.12.023>.

- 36 Bojack A, Zhao L, Morris PF, Sietsma J. In-situ determination of austenite and martensite formation in 13Cr6Ni2Mo supermartensitic stainless steel. *Materials Characterization*. 2012;71:77-86. <http://doi.org/10.1016/j.matchar.2012.06.004>.
- 37 Carvalho LG, Andrade MS, Plaut RL, Souza FM, Padilha AF. A dilatometric study of the phase transformations in 300 and 350 maraging steels during continuous heating rates. *Materials Research*. 2013;16(4):740-744. <http://doi.org/10.1590/S1516-14392013005000069>.
- 38 García de Andrés C, Caballero FG, Capdevila C, Álvarez LF. Application of dilatometric analysis to the study of solid–solid phase transformations in steels. *Materials Characterization*. 2002;48(1):101-111. [http://doi.org/10.1016/S1044-5803\(02\)00259-0](http://doi.org/10.1016/S1044-5803(02)00259-0).
- 39 Electro Optical Systems – EOS GmbH. Material data sheet EOS MaragingSteel MS1. Vol. 49. München: EOS; 2011.
- 40 Santos PLL, Avila JA, Fonseca EB, Gabriel AHG, Jardini AL, Lopes ÉSN. Plane-strain fracture toughness of thin additively manufactured maraging steel samples. *Additive Manufacturing*. 2022;49:102509. <http://doi.org/10.1016/j.addma.2021.102509>.
- 41 Dehgahi S, Ghoncheh MH, Hadadzadeh A, Sanjari M, Amirkhiz BS, Mohammadi M. The role of titanium on the microstructure and mechanical properties of additively manufactured C300 maraging steels. *Materials & Design*. 2020;194:108965. <http://doi.org/10.1016/j.matdes.2020.108965>.
- 42 Jäggle E, Sheng Z, Kürnsteiner P, Ocylok S, Weisheit A, Raabe D. Comparison of maraging steel micro- and nanostructure produced conventionally and by laser additive manufacturing. *Materials*. 2016;10(1):8. <http://doi.org/10.3390/ma10010008>.
- 43 Morsdorf L, Jeannin O, Barbier D, Mitsuhashi M, Raabe D, Tasan CC. Multiple mechanisms of lath martensite plasticity. *Acta Materialia*. 2016;121:202-214. <http://doi.org/10.1016/j.actamat.2016.09.006>.
- 44 Król M, Snopiński P, Czech A. The phase transitions in selective laser-melted 18-Ni (300-grade) maraging steel. *Journal of Thermal Analysis and Calorimetry*. 2020;142(2):1011-1018. <http://doi.org/10.1007/s10973-020-09316-4>.
- 45 Peters DT. A study of austenite reversion during aging of maraging steels. *Trans ASM*. 1968;61:62-74.
- 46 Guo Z, Sha W. Modelling the correlation between processing parameters and properties of maraging steels using artificial neural network. *Computational Materials Science*. 2004;29(1):12-28. [http://doi.org/10.1016/S0927-0256\(03\)00092-2](http://doi.org/10.1016/S0927-0256(03)00092-2).
- 47 Padial AGF. Caracterização microestrutural do aço maraging de grau 400 de resistência mecânica ultra-elevada [tese]. São Paulo: Universidade de São Paulo; 2002.
- 48 Banerjee BR, Hauser JJ, Capenos JM. Role of cobalt in the marage-type alloy matrix. *Metal Science Journal*. 1968;2(1):76-80. <http://doi.org/10.1179/030634568790443125>.
- 49 Niu MC, Yin LC, Yang K, Luan JH, Wang W, Jiao ZB. Synergistic alloying effects on nanoscale precipitation and mechanical properties of ultrahigh-strength steels strengthened by Ni₃Ti, Mo-enriched, and Cr-rich co-precipitates. *Acta Materialia*. 2021;209:116788. <http://doi.org/10.1016/j.actamat.2021.116788>.
- 50 Tan C, Zhou K, Kuang M, Ma W, Kuang T. Microstructural characterization and properties of selective laser melted maraging steel with different build directions. *Science and Technology of Advanced Materials*. 2018;19(1):746-758. <http://doi.org/10.1080/14686996.2018.1527645>.
- 51 Alves TJB, Nunes GCS, Tupan LFS, Sarvezuk PWC, Ivashita FF, Oliveira CAS, et al. Aging-induced transformations of maraging-400 alloys. *Metallurgical and Materials Transactions. A, Physical Metallurgy and Materials Science*. 2018;49(8):3441-3449. <http://doi.org/10.1007/s11661-018-4724-y>.
- 52 Niu M, Zhou G, Wang W, Shahzad MB, Shan Y, Yang K. Precipitate evolution and strengthening behavior during aging process in a 2.5 GPa grade maraging steel. *Acta Materialia*. 2019;179:296-307. <http://doi.org/10.1016/j.actamat.2019.08.042>.
- 53 Rohit B, Muktinutalapati NR. Fatigue behavior of 18% Ni maraging steels: a review. *Journal of Materials Engineering and Performance*. 2021;30(4):2341-2354. <http://doi.org/10.1007/s11665-021-05583-w>.
- 54 Floreen S, Hayden HW. Some observations of void growth during the tensile deformation of a high strength steel. *Scripta Metallurgica*. 1970;4(2):87-94. [http://doi.org/10.1016/0036-9748\(70\)90170-5](http://doi.org/10.1016/0036-9748(70)90170-5).
- 55 Kalish D, Rack HJ. Thermal embrittlement of 18 Ni(350) maraging steel. *Metallurgical Transactions*. 1971;2(9):2665-2672. <http://doi.org/10.1007/BF02814910>.
- 56 Psioda JA, Low JR Jr. The effect of microstructure and strength on the fracture toughness of an 18 Ni, 300 grade maraging steel. Washington, D.C.: NASA; 1977.

Dilatometric insights into classical and modern maraging steels: a comparative analysis of grades 300, 350, and 400

Received: 1 Feb. 2024

Accepted: 17 Oct. 2024

Editor-in-charge: André Luiz Vasconcellos da Costa e Silva - 